JOURNAL OF AIRCRAFT
Vol. 43, No. 2, March–April 2006

Swashplateless Helicopter Rotor with Trailing-Edge Flaps for Flight and Vibration Control

Jinwei Shen*
National Institute of Aerospace, Hampton, Virginia 23666
Mao Yang†
Northwestern Polytechnical University, Xi'an 710072, People's Republic of China
and
Inderjit Chopra‡
University of Maryland, College Park, Maryland 20742

The objective of this study is to demonstrate the concept of active trailing-edge flaps as primary flight control and vibration reduction devices for a typical full-scale helicopter. A comprehensive rotorcraft analysis based on UMARC was developed to analyze the swashplateless rotor. A parametric study of various key design variables involved in the trailing-edge flap design was carried out. An optimal design of a trailing-edge flap system that provides effective control authority within the complete range of advance ratios as well as minimum actuation requirements was achieved. Trailing-edge flaps demonstrated the capability of performing both primary flight control and active vibration control functions. At a high forward speed (advance ratio of 0.32), the 4/rev vertical force and roll and pitch moments at hub are successfully eliminated (by 90%), and the 4/rev in-plane hub forces are reduced by more than 40%. The half peak-to-peak value of the trailing-edge flap deflection for primary flight control is 7.1 deg, and an additional 4.7 deg is required for active vibration control.

Nomenclature

c	=	airfoil chord length
c_b	=	trailing-edge flap nose overhang length
F_x	=	N_b/rev longitudinal vibratory hub force
F_y	=	N_b/rev lateral vibratory hub force
F_z	=	N_b/rev vertical vibratory hub force
J	=	scalar nondimensional vibration objective function
M_h	=	trailing-edge flap hinge moment
M_x	=	N_b/rev roll vibratory hub moment
M_y	=	N_b/rev pitch vibratory hub moment
N_b	=	number of rotor blades
P_f	=	trailing-edge flap actuation power
W_z	=	weighting matrix for hub loads
$W_{\Delta\theta}$	=	weighting matrix for flap control input rates
W_θ	=	weighting matrix for flap control inputs
z	=	vector of components of hub loads
δ	=	trailing-edge flap deflection (positive flap down)
δ_0	=	trailing-edge flap collective deflection
δ_{1c}	=	trailing-edge flap lateral cyclic deflection
δ_{1s}	=	trailing-edge flap longitudinal cyclic deflection
$\dot{\delta}$	=	trailing-edge flap rate
θ	=	blade section pitch (positive nose upward)
θ_{index}	=	blade-pitch index angle (positive nose upward)
θ_{root}	=	blade-pitch motion at root spring (positive nose upward)
μ	=	advance ratio
ψ	=	azimuth angle

Subscripts

$0, 1c, 1s, \ldots,$ pc, ps, $\ldots, \infty$	=	harmonics of a sine/cosine Fourier series representation of a periodic function

Introduction

THE use of trailing-edge flaps for primary flight control started as early as 1922 when Pescara incorporated plain flaps for blade pitch control.[1] The trailing-edge flap provides blade-pitch change indirectly as a result of aerodynamic pitching-moment variation with trailing-edge flap deflections. However, because of the inherent mechanical complexity, the trailing-edge flap mechanism has not been widely adopted by rotorcraft industry with the exception of Kaman helicopters.[2] With the recent emergence of high-energy density smart material actuators, it appears that active trailing-edge flaps might become a feasible solution to blade-pitch control.[3] The use of a trailing-edge flap for primary flight control appears attractive in the context of an actively controlled rotor, where the embedded flaps can perform multiple functions. Experiments conducted by Barrett et al.[4] on a model scale helicopter achieved a 26% reduction in parasite drag, 40% reduction in flight control system weight, and 8% reduction in total aircraft gross weight by eliminating the swashplate assembly. Furthermore, as an additional capability, the use of active trailing-edge flaps to reduce helicopter vibration and noise has been shown through numerical simulations.[5–9]

The present study exploits the ability of trailing-edge flaps to produce aerodynamic pitching moments in order to provide swashplateless primary flight control. Aerodynamic blade pitching moments, produced by deflecting the trailing-edge flap, impel rotor blade to pitch against the root spring to achieve aerodynamic equilibrium. There are primarily two types of flaps: servo flaps and plain flaps. The servo-flap design consists of an auxiliary airfoil section that is located aft of the trailing edge of the main blade. Despite the successful service history of servo flaps for primary flight control on helicopters built by Kaman,[2,10] plain flaps are the choices of most of the recently developed actively controlled rotors[9,11–13] because plain flaps can be easily coupled with the smart material actuators. In such a configuration, the flap is integrated into the rotor blade by locating the flap actuation and support structure, hinge, and linkage assembly within the blade profile, resulting in a minimum aerodynamic drag. Also, by narrowing the hinge gap, the flap effectiveness

Presented as Paper 2004-1951 at the AIAA/ASME/ASCE/AHS/ASC 45th Structures, Structural Dynamics and Materials Conference, Palm Springs, CA, 19–22 April 2004; received 17 November 2004; revision received 1 July 2005; accepted for publication 1 July 2005.

*Research Scientist. Member AIAA.
†Associate Professor.
‡Alfred Gessow Professor and Director. Fellow AIAA.

can be increased. However, the plain flaps are located much closer to the blade elastic axis compared to the servo-flap configurations; hence, their capability to generate pitching moment is smaller. In this study, plain trailing-edge flaps are investigated as a device for primary flight and vibration control.

In a recent study, the authors developed a comprehensive aeromechanics analysis[14] based on UMARC (University of Maryland Advanced Rotorcraft Code)[15] for a swashplateless rotor with trailing-edge flaps. The analysis was carried out for a five-bladed bearingless rotor system (MD900) with a soft pitch link (control frequency of 2.1/rev) trimmed to wind-tunnel trim conditions. A swashplateless rotor with plain flaps was shown to trim successfully in the complete range of advance ratios examined. Furthermore, the required trailing-edge flap angles were found to be moderate dependent on a proper selection of blade-pitch index angle. A multicyclic controller was implemented to minimize vibratory hub loads with the swashplateless rotor system. The plain flaps were shown to be capable of performing both primary flight control and active vibration control functions. Additionally, the authors conducted a parametric study[16] for this swashplateless design. Blade-pitch index angle, blade-root spring stiffness, and trailing-edge flap location and size (length and chord ratio) were found to be key design parameters. In addition, the aeroelastic stability characteristics were compared between the swashplateless rotor and conventional swashplate rotor. Overall, the swashplateless rotor was found to be more stable than the conventional rotor. More recently, the authors[17] developed a comprehensive rotorcraft analysis to examine plain trailing-edge flaps for primary flight control of an ultralight helicopter (ASI496) with two-bladed teetering rotor. Again, the requirements for trailing-edge flap angles were found moderate for the complete range of advance ratios. The study was then extended to examine the actuation requirements of a trailing-edge flap system as a primary flight control device for an ultralight helicopter rotor in maneuvering flight and autorotation.[18]

The preceding studies were carried out using baseline rotors of ultralight and lightweight helicopters. However, the benefit of replacing a conventional swashplate system with trailing-edge flaps might be more significant when applied to a medium- to large-weight helicopter. Furthermore, the actuation requirements of a trailing-edge flap system of such a helicopter might be more stringent because of the higher control authority requirements. Therefore, the present study uses the rotor of a full-scale utility helicopter, the Black-Hawk (UH-60), as the baseline rotor. The objectives of this study are to 1) investigate the trailing-edge flap concept for primary flight and active vibration control for a full-scale utility helicopter, 2) carry out a parametric design study that identifies key design variables to minimize actuation requirements, and 3) select an optimal trailing-edge flap system that provides sufficient control authority with minimum actuation requirements.

Analytical Model

The baseline rotor for the swashplateless configuration is the UH-60 rotor (Table 1). The rotor utilizes a four-bladed articulated rotor design and has a normal gross weight of 19,000 lb. The conventional swashplate control system places the rotating blade torsional frequency around 4.0/rev (Ref. 19). Because the swashplateless rotor must be designed with torsionally soft blades in order to reduce control actuation forces of the trailing-edge flap system, the present swashplateless rotor design modifies the baseline rotor by replacing the pitch link assembly with a soft linear root spring, thereby reducing the torsional frequency to 1.9/rev.

Table 1 Rotor properties

Property	Value
Rotor type	Articulated
Number of blades	4
Rotor radius	26.8 ft
Rotor speed	258 rpm
Solidity	0.0826
Lock number	8
Gross weight	19,000 lb
Root cutout	14%
Twist angle	−18 deg

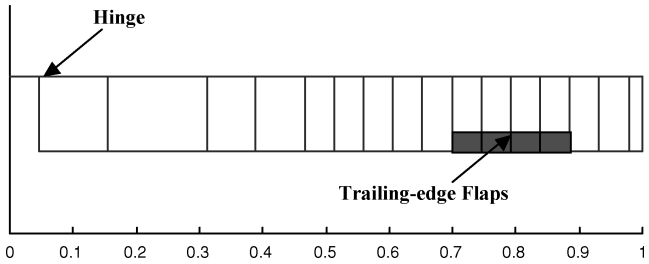

Fig. 1 Blade and flap discretization.

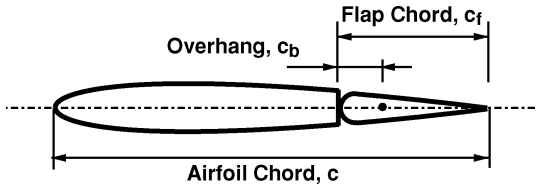

Fig. 2 Trailing-edge flap with aerodynamic balance (nose overhang).

The baseline rotor analysis is adapted from UMARC. The modeling of the swashplateless rotor with trailing-edge flaps in free flight steady trim is discussed in Ref. 20. The following briefly outlines the analysis and solution procedure. The analysis incorporates finite element methodology in space and time. The blade is modeled as an elastic beam undergoing flap bending, lag bending, elastic twist, and axial deformation. The rotor blades are discretized into a finite number of beam elements, each with 15 deg of freedom. Sixteen aerodynamic/structural elements are used to model the main blade (Fig. 1). The Drees linear inflow is used to obtain the induced inflow distribution over the rotor disk. The coupled blade response and the trim control settings are solved simultaneously for a propulsive trim condition. Eight time elements with fifth-order shape functions are used to calculate a coupled trim solution. The trailing-edge flap motion is prescribed, and as such, actuator dynamics are neglected for this study.[21] However, trailing-edge flap aerodynamic and inertial effects are included both in the formulation of the blade equations of motion and the computation of hub loads. A quasi-steady model adapted from Theodorsen's theory[22] is used to model the aerodynamically balanced flap (Fig. 2). This model considers the gap sealed, that is, no leakage of fluid between the flap and the base airfoil.

For a swashplateless rotor with trailing-edge flaps, the flaps produce pitching-moment changes, which in turn pitch the main rotor blades, thereby producing the desired collective and cyclic blade pitch. The trim variables for a swashplateless rotor are flap collective deflection δ_0 and flap cyclic deflections δ_{1c} and δ_{1s}. The control angle input to the trailing-edge flap is given by

$$\delta(\psi) = \delta_0 + \delta_{1c}\cos\psi + \delta_{1s}\sin\psi \tag{1}$$

and the blade-pitch angle consists of the blade-pitch index angle plus the pitch induced by flap control inputs,

$$\theta(\psi) = \theta_{\text{index}} + \theta_{\text{root}}(\psi) \tag{2}$$

It is attractive to use trailing-edge flaps for both primary flight and active vibration control in order to reduce overall system weight, complexity, and cost. Trailing-edge flap actuation required to minimize N_b/rev fixed system hub loads occurs at higher harmonics of rotational speed, typically at $(N_b - 1, N_b, N_b + 1)$/rev. For active vibration control, the trailing-edge flap input is given by

$$\delta(\psi) = \sum_p [\delta_{\text{pc}}\cos(p\psi) + \delta_{\text{ps}}\sin(p\psi)] \tag{3}$$

where $p = N_b - 1, N_b, N_b + 1$. For a four-bladed rotor used in the present study, the trailing-edge flap inputs are 3, 4, and 5/rev. A multicyclic controller[23] is used to determine the flap control inputs (δ_{pc}, δ_{ps}). This algorithm is based on the minimization of an objective function,

$$J \equiv z_n^T W_z z_n + \theta_n^T W_\theta \theta_n + \Delta\theta_n^T W_{\Delta\theta} \Delta\theta_n \tag{4}$$

where z_n is a hub loads vector containing the cosine and sine coefficients of the N_b/rev fixed system hub loads F_x, F_y, F_z, M_x, and M_y at iteration n. θ_n and $\Delta\theta_n$ represent the harmonics of the control inputs and control rates, respectively. The diagonal matrices W contain weights for different harmonics of the vibration W_z, the control inputs W_θ, and the control rates $W_{\Delta\theta}$.

By superimposing the input for primary flight control, the control input to the flap is

$$\delta(\psi) = \delta_0 + \delta_{1c}\cos(\psi) + \delta_{1s}\sin(\psi) + \sum_p [\delta_{pc}\cos(p\psi) + \delta_{ps}\sin(p\psi)] \tag{5}$$

The actuation power of the flap system is calculated by integrating the product of the hinge moment and flap deflection rate over one complete rotor revolution:

$$P_f = \frac{N_b}{2\pi}\int_0^{2\pi} \max(-M_h\dot{\delta}, 0)\, d\psi \tag{6}$$

The actuation power presented in Eq. (6) is "ideal" because it only includes the energy used to drive the flap system and neglects other power consumptions, such as the heat dissipation of the smart actuators.

Results and Discussion

The baseline trailing-edge flap characteristics are given in Table 2. In the present study, flap nose-up displacement represents positive control angle.

Preliminary Trailing-Edge Flap Performance

Figure 3 shows the control angles, hinge moment, and the actuation power of the trailing-edge flap required for trimmed flight at different forward speeds. Figure 3a shows the flap control angles δ_0, δ_{1c}, and δ_{1s} as a function of flight speed. Results show that δ_{1c} varies with speed in a narrow range (from -1.3 to 3 deg). The collective flap angle δ_0 remains positive (nose up) for flight speeds up to an advance ratio of 0.25, above which negative δ_0 (nose down) resulting in a reduction of net lift. Results also reveal that δ_{1s} is large at advance ratios above 0.25 because of the adverse cyclic effect caused by a nose-up δ_0 in forward flight conditions. The trailing-edge flap half peak-to-peak angle is defined as $\sqrt{(\delta_{1c}^2 + \delta_{1s}^2)}$. Based on this preliminary design, smart material actuators might not be able to achieve such large half peak-to-peak flap angles. (At advance ratio of 0.32, the half peak-to-peak angle is 18 deg.) Thus, there is a need to search for another design solution. Figure 3b shows the total flap hinge moment and actuation power as a function of airspeed. The flap hinge moment is shown in terms of both mean and half peak-to-peak values. The half peak-to-peak hinge moment is shown to increase with airspeed; however, the mean value is less sensitive to airspeed. The actuation power increases with airspeed.

Table 2 Baseline and optimized trailing-edge flap rotor characteristics

Property	Baseline	Optimized
Flap type	Plain flap	Plain flap
Blade-pitch index angle	10 deg	14.5 deg
Flap length	19%R	28%R
Flap chord ratio	25%c	15%c
Flap location	80%R	80%R
Flap hinge overhang	0	5%c

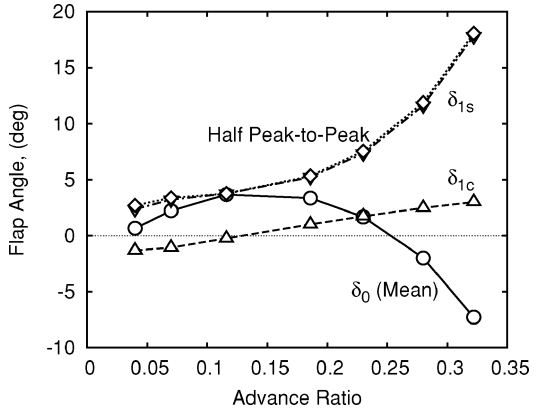

a) Trailing-edge flap angle

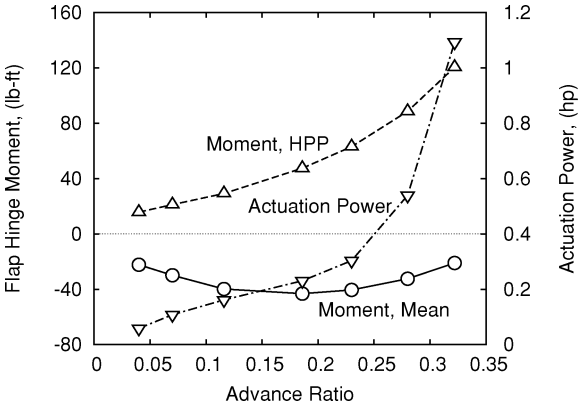

b) Flap hinge moment and actuation power

Fig. 3 Trailing-edge flap deflection and actuation requirements of baseline swashplateless rotor at different forward speeds.

Below advance ratio of 0.28, the power required is below 0.54 hp. However, when speed increases from advance ratio of 0.28 to 0.32, the power requirement jumps to 1.1 hp. The reason for this jump in power might be the combination of large flap control angles and large hinge moments required to overcome at high speeds.

The preliminary design demonstrated the capability of using trailing-edge flaps to trim the rotor. However, results show that at a high speed, such as an advance ratio of 0.32, the control angles become quite large, which might not be feasible with current smart material actuators. Furthermore, the large trailing-edge flap deflections coupled with large flap hinge moments result in excessive required actuation power at high flight speeds. Therefore, the preliminary design needs to be improved to reduce the trailing-edge flap actuation requirements.

Parametric Study

An assessment of the preliminary design indicates that the trailing-edge flap performance is less satisfactory at high speeds. To improve the performance, a parametric study is carried out to optimize the flap design at a high flight speed condition (advance ratio of 0.32). Selected parameters are 1) trailing-edge flap overhang, 2) flap size (length and chord ratio), 3) flap spanwise location, and 4) blade-pitch index angle. The performance of the preliminary design is referred to as baseline configuration. During the parametric study, only one parameter is changed while others are kept constant.

The flap nose overhang c_b is defined as the hinge offset from the leading edge of the flap (see Fig. 2). The flap nose overhang is often referred to as a flap aerodynamic balance. By moving the flap hinge aft, that is, $c_b > 0$, the flap hinge moment can be reduced. In the baseline configuration, there is no overhang, resulting in a large flap hinge moment (Fig. 3b). Figure 4a shows the effect of the flap overhang on flap control angles at advance ratio of 0.32. The results indicate that the flap control angles decrease when the flap overhang is increased because of the increased sensitivities of

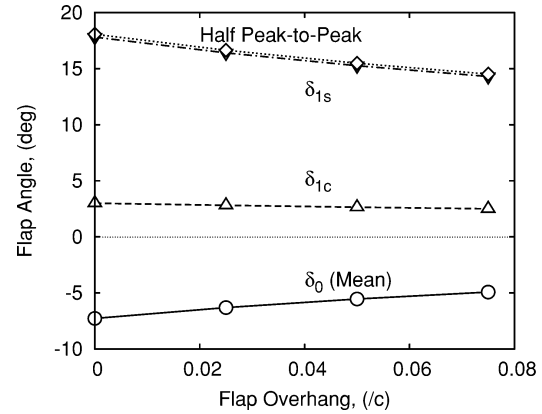

a) Trailing-edge flap angle

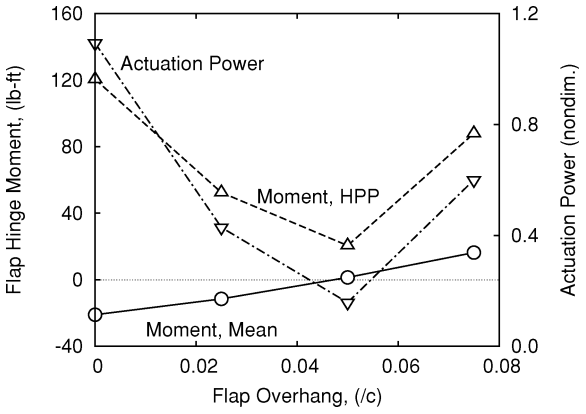

b) Flap hinge moment and actuation power

Fig. 4 Effect of flap overhang on flap deflection and actuation requirements ($\mu = 0.32$).

pitching moment to flap angle. The reduction in flap control angles is beneficial to the design. Figure 4b shows the effect of flap overhang on actuation power and flap hinge moment (mean and half peak-to-peak values). Significant reductions in hinge moments and actuation power are archived by increasing the flap overhang from 0 to 5% of chord length. Further increases in the flap overhang result in the growth of hinge moments and actuation power. Results indicate that the optimum overhang is 5% of chord length.

Figure 5a shows the flap control angles as a function of flap length. The flap control angles are shown to decrease as flap length increases because large flap generates large control forces at same control angle. Figure 5b shows that the half peak-to-peak hinge moment decreases with flap length while the steady part increases with flap length. This reduction of the half peak-to-peak value translates into a reduction in actuation power. Figure 5 indicates that by increasing the flap length the flap performance improves. These figures show that the reductions in control angles, flap hinge moments, and actuation power are most significant when the flap length is increased from 19%R to 28%R. Considering that 1) when the flap is extended toward the tip, the tip losses can affect flap performance; and 2) it is preferable to have a compact trailing-edge flap, 28%R seems to be a better choice for the flap length. The flap control angle (half peak-to-peak) is still quite high (approximate 10 deg) even when the flap length is 28%R.

Another parameter used to determine the flap size is the flap chord ratio (Fig. 2). Figure 6a shows the flap control angles are not very sensitive to flap chord ratio because of the small changes of sensitivities of pitching moment to flap deflection in the flap chord range of 0.1c to 0.25c. Figure 6b shows that the actuation power and flap hinge moment (both steady and half peak-to-peak values) increase with flap chord ratio.

Another design parameter is the spanwise location of trailing-edge flap. Figure 7a shows the effect of trailing-edge flap location on flap angles at an advance ratio of 0.32. The flap angles decrease

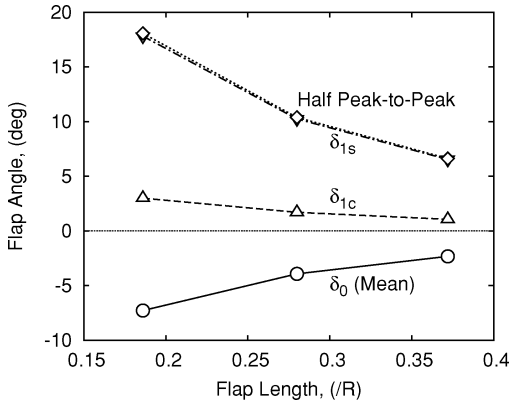

a) Trailing-edge flap angle

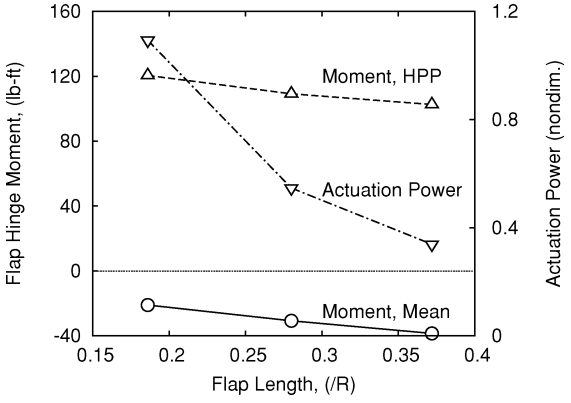

b) Flap hinge moment and actuation power

Fig. 5 Effect of flap length on flap deflection and actuation requirements ($\mu = 0.32$).

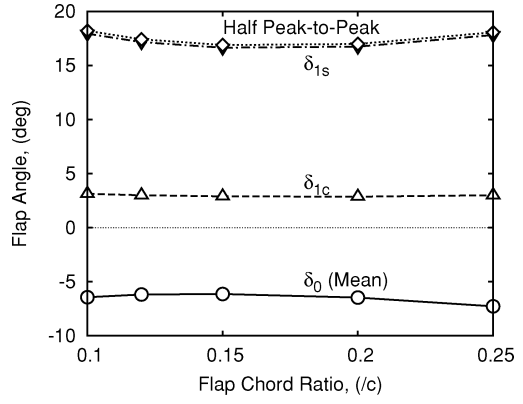

a) Trailing-edge flap angle

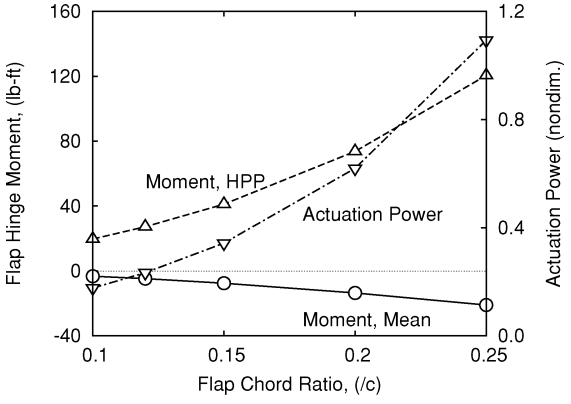

b) Flap hinge moment and actuation power

Fig. 6 Effect of flap chord ratio on flap deflection and actuation requirements ($\mu = 0.32$).

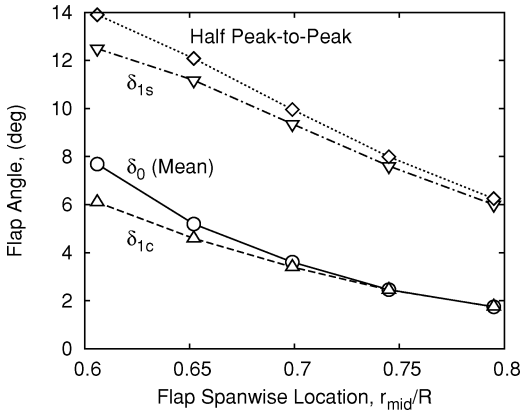

a) Trailing-edge flap angle

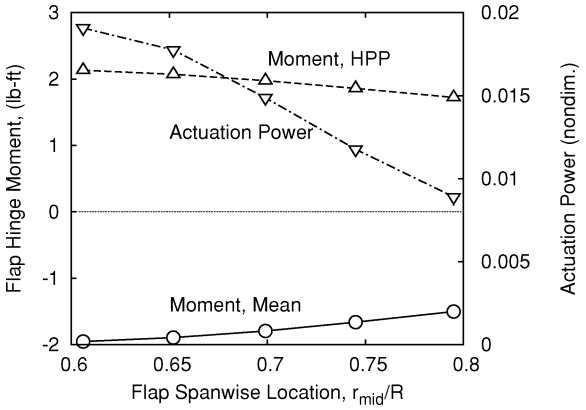

b) Flap hinge moment and actuation power

Fig. 7 Effect of flap spanwise location on flap deflection and actuation requirements (blade-pitch index angle of 14.5 deg, $\mu = 0.32$).

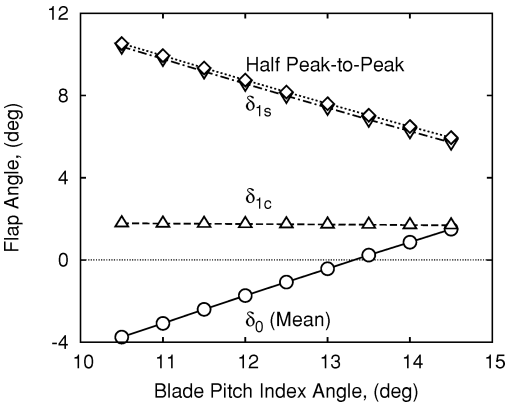

a) Trailing-edge flap angle

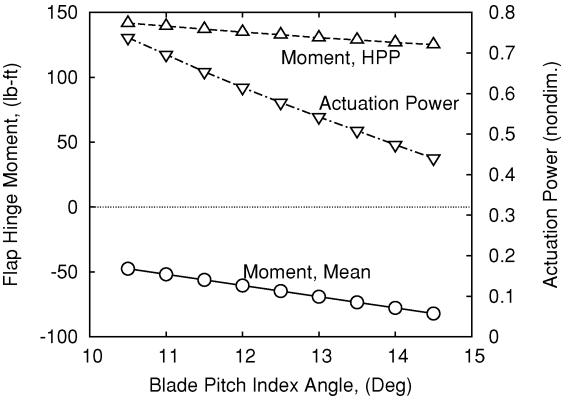

b) Flap hinge moment and actuation power

Fig. 8 Effect of blade-pitch index angle on flap deflection and actuation requirements (flap overhang of 0.05c, $\mu = 0.32$).

when the flap is located close to the blade tip, where high dynamic pressure exists. Figure 7b shows that the actuation power and flap hinge moment are reduced when the flap is located near the tip.

The final variable examined is the blade-pitch index angle, a precollective angle used to reduce the control requirements. Figure 8a shows that δ_{1s} decreases when the pitch index angle increases while δ_{1c} is insensitive to this change. The longitudinal cyclic flap deflections reduce because of the favorable blade cyclic pitch effect induced by downward flap collective deflection δ_0 in the asymmetric aerodynamic environment at forward flight. It is also noteworthy that δ_0 becomes positive when the pitch index angle exceeds 13.5 deg and generates upward lift on the blade. This upload moves the blade airload distribution inboard and improves the rotor performance in hover and forward flight conditions.[24] The half peak-to-peak flap deflections reduce from 10.5 to 6 deg when a pitch index angle of 14.5 deg is used instead of the baseline 10 deg. Figure 8b shows that the actuation power also decreases as the pitch index angle increases because of the reductions of hinge moment (half peak to peak). Based on this parametric study, a larger blade-pitch index angle should be used.

Optimized Trailing-Edge Flap Design

The performance of the preliminary design is not satisfactory at high speeds. Based on the parametric study conducted at a high-speed forward-flight condition ($\mu = 0.32$), the design parameters of the flap are adjusted in order to increase the trailing-edge flap effectiveness as well as to decrease the actuation requirements. Table 2 compares the parameters of the baseline and optimized designs. The performance of the baseline and optimized designs will next be compared at various airspeeds.

Figure 9 presents the comparison of the flap control angles (δ_0, δ_{1c}, δ_{1s}) at different advance ratios. With an increase in the pitch index angle from 10 to 14.5 deg, the collective flap control angle becomes positive, flap nose up at all airspeeds examined (Fig. 9a), which

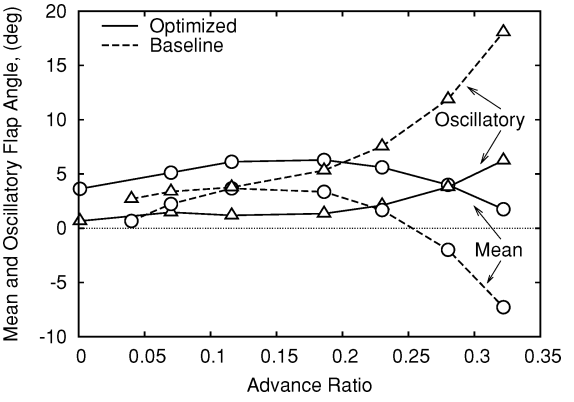

a) Mean and oscillatory flap angle

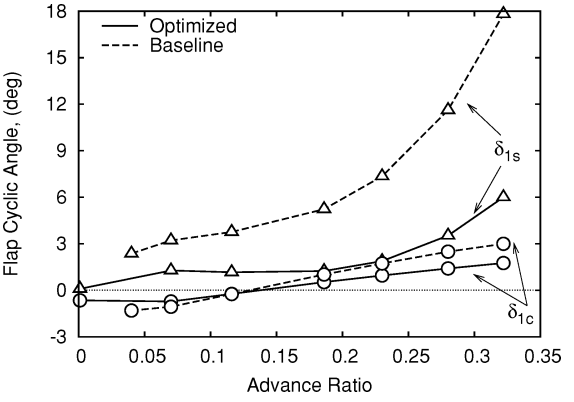

b) Flap cyclic angle

Fig. 9 Comparison of flap angles of baseline and optimized trailing-edge flap configurations ($\mu = 0.32$).

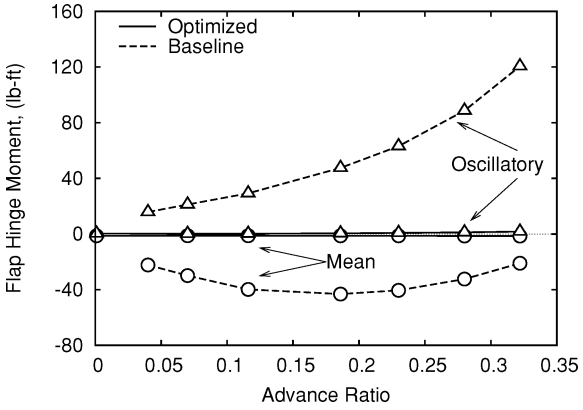

a) Flap hinge moment

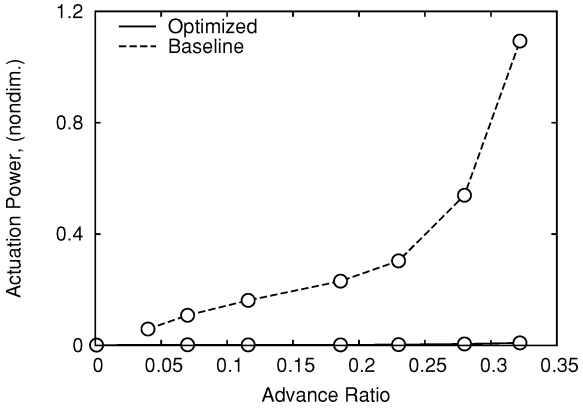

b) Flap actuation power

Fig. 10 Comparison of actuation requirements of baseline and optimized trailing-edge flap configurations ($\mu = 0.32$).

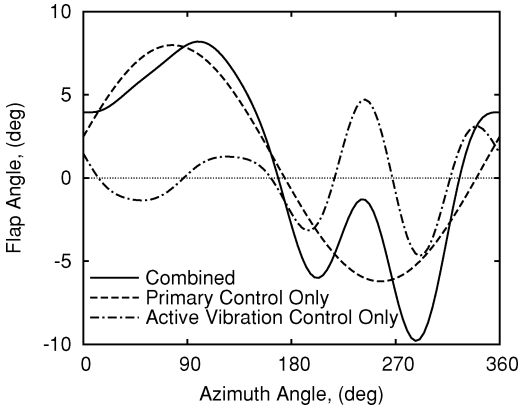

a) Flap angle

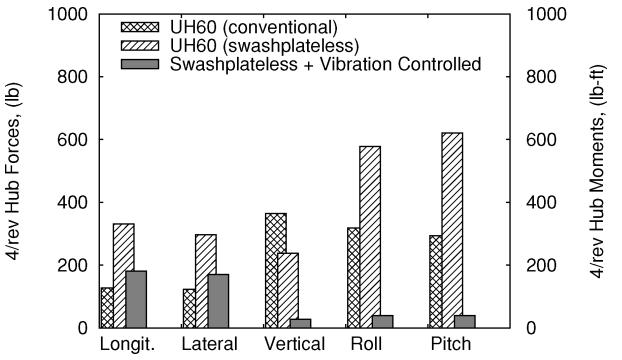

b) 4/rev vibratory hub load minimization

Fig. 11 Trailing-edge flap performing both primary flight and vibration control ($\mu = 0.32$).

benefits the rotor performance because the flaps generate positive lift. The range of the collective flap angle is also kept between 2 to 6 deg. Furthermore, the collective flap control angle is only 2 deg instead of −7.8 deg at high advance ratio of 0.32. Figure 9b shows that compared to the baseline design the optimized design reduces the lateral cyclic flap control angle δ_{1c} at all speeds. Likewise, the longitudinal cyclic control angle δ_{1s} for the optimized design is significantly lower than the baseline; in fact, the maximum value of δ_{1s} is now 6 deg instead of 18 deg.

Figure 10 shows the comparison of flap actuation requirements at different flight speeds. Figure 10a shows the steady and half peak-to-peak components of the flap hinge moment, respectively. As expected, the optimized design reduces the flap hinge moment significantly compared to the baseline configuration. Figure 10b shows that the flap actuation power of the optimized design is minimized substantially compared to the baseline. The actuation power reduction is primarily attributed to the incorporation of the aerodynamic balance (flap nose overhang), which results in a reduction in the hinge moment.

Primary Flight and Vibration Control

Predictions with a trailing-edge flap performing both primary flight control and active vibration control are shown in Fig. 11. The optimized trailing-edge flap design is used in this simulation. Figure 11a illustrates the flap input required to provide both primary flight control and active vibration control for a complete rotor revolution at an advance ratio of 0.32. The total flap inputs required for both primary flight control and active control are between −10 and 8 deg. The half peak-to-peak flap control angle for primary flight control is 7.1 deg, and an additional 4.7 deg is required for active vibration control. Figure 11b compares the 4/rev vibratory hub loads of three rotor configurations: the conventional swashplate control rotor, the swashplateless rotor without active flap inputs for vibration reduction, and the swashplateless rotor with active vibration control. For the rotor with active vibration control, the weighting parameters on the hub loads are {0.04, 0.023, 1.0, 126.04, 38.96}, acting on hub longitudinal, lateral, and vertical forces, and rolling and pitching moments, respectively. The large weightings on the vertical force and the rolling and pitching moments in the objective function result in a 90% reduction in the 4/rev components of these hub loads. The longitudinal and lateral hub forces are reduced respectively to 57 and 59% of uncontrolled values.

Conclusions

The concept of trailing-edge flaps as primary flight control as well as active vibration control for a full-scale utility helicopter (UH-60) was investigated. A parametric study of various key design variables involved in the trailing-edge flap design was carried out. An optimized design of the trailing-edge flap system that provides effective control authority within the examined flight envelope as well as minimum actuation requirements was achieved. Based on this study, some conclusions can be drawn:

1) By properly selecting the blade-pitch index angle, the flap control angles are reduced. At an advance ratio of 0.32, the half peak-to-peak trailing-edge flap deflections reduce from 10.5 to 6 deg.

2) Increasing flap spanwise length reduces the flap control angles. When the flap length increases from 19%R to 28%R, the half peak-to-peak flap angle decreases from 17 to 10 deg at an advance ratio of 0.32.

3) Flap overhang length significantly affects flap actuation power and hinge moment. A 5%c flap overhang reduces the actuation power to 0.2 hp from 1.1 hp.

4) The optimized design of the trailing-edge flap system, consisting of a 28%R plain flap with 15%c chord ratio and 5%c overhang and located at the 80%R position, requires moderate flap control angles to trim the rotor throughout the complete range of the flight speeds examined. The collective and cyclic flap angles are less than 6 deg, and the actuation power requirements are also small.

5) Trailing-edge flaps are shown to be capable of performing both primary flight control and active vibration control functions. The

4/rev vertical force, roll, and pitch moments at hub are minimized at an advance ratio of 0.32 (90% reductions). The 4/rev in-plane hub forces are reduced by more than 40%. The half peak-to-peak value of the trailing-edge flap deflection for primary flight control is 7.1 deg, and an additional 4.7 deg is required for active vibration control.

Overall, the observed trends of various design parameters on actuation requirements of trailing-edge flap for primary flight control of the medium/heavy utility helicopter (UH60) are similar to previous studies on light (MD900) and ultralight (ASI496). However, the required flap actuation power of a UH60 trailing-edge flap system is the largest, as expected.

Acknowledgments

This work was supported by U.S. Army AMCOM, AMRDEC in Huntsville, Alabama, with John Berry as technical monitor. This work was carried out as an SBR contract to System Planning and Analysis, Inc. (SPA) with Jason Kiddy as principal investigator. We also appreciate useful additional comments from Martin Sekula (U.S. Army Research Laboratory, Vehicle Technology Directorate).

References

[1]Pescara, R., "Screw Propeller of Helicopter Flying Machines," U.S. Patent 1,449,129, March 1923.

[2]Kaman, C., "Aircraft of Rotary Wing Type," U.S. Patent 2,455,866, Dec. 1948.

[3]Chopra, I., "Status of Application of Smart Structures Technology to Rotorcraft Systems," *Journal of the American Helicopter Society*, Vol. 45, No. 4, 2000, pp. 228–252.

[4]Barrett, R., Schliesman, M., and Frye, P., "Design, Development and Testing of a Mini Solid State Adaptive Rotorcraft," *SPIE Symposium on Smart Structures and Materials, Conference on Smart Structures and Integrated Systems*, edited by M. E. Regelbrugge, Vol. 3041, Society of Photo-Optical Instrumentation Engineers, Bellingham, WA, 1997, pp. 231–242.

[5]Friedmann, P., and Millott, T., "Vibration Reduction in Rotorcraft Using Active Control: A Comparison of Various Approaches," *Journal of Guidance, Control, and Dynamics*, Vol. 18, No. 4, 1995, pp. 664–673.

[6]Milgram, J., Chopra, I., and Straub, F., "Rotors with Trailing Edge Flaps: Analysis and Comparison with Experimental Data," *Journal of the American Helicopter Society*, Vol. 43, No. 4, 1998, pp. 319–332.

[7]Milgram, J., and Chopra, I., "A Parametric Design Study for Actively Controlled Trailing Edge Flaps," *Journal of the American Helicopter Society*, Vol. 43, No. 2, 1998, pp. 110–119.

[8]Myrtle, T. F., and Friedmann, P. P., "Vibration Reduction in Rotorcraft Using Actively Controlled Trailing Edge and Issue Related to Practical Implementation," *AHS International 54th Annual Forum Proceedings*, American Helicopter Society, Alexandria, VA, 1998, pp. 602–619.

[9]Straub, F. K., and Charles, B. D., "Aeroelastic Analysis of Rotors with Trailing Edge Flaps Using Comprehensive Codes," *Journal of the American Helicopter Society*, Vol. 46, No. 3, 2001, pp. 192–199.

[10]Wei, F.-S., and Jones, R., "Correlation and Analysis for SH-2F 101 Rotor," *Journal of Aircraft*, Vol. 25, No. 7, 1988, pp. 647–652.

[11]Fulton, M. V., and Ormiston, R. A., "Hover Testing of a Small-Scale Rotor with on-Blade Elevons," *Journal of the American Helicopter Society*, Vol. 46, No. 2, 2001, pp. 96–106.

[12]Bernhard, A., and Chopra, I., "Trailing Edge Flap Activated by a Piezo-Induced Bending-Torsion Coupled Beam," *Journal of the American Helicopter Society*, Vol. 44, No. 1, 1999, pp. 3–15.

[13]Koratkar, N. A., and Chopra, I., "Wind Tunnel Testing of a Mach-Scaled Rotor Model with Trailing-Edge Flaps," *Smart Materials and Structures*, Vol. 10, No. 1, 2001, pp. 1–14.

[14]Shen, J., and Chopra, I., "Swashplateless Helicopter Rotor with Trailing-Edge Flaps," *Journal of Aircraft*, Vol. 41, No. 2, 2004, pp. 208–214.

[15]Bir, G., and Chopra, I., "University of Maryland Advanced Rotor Code (UMARC) Theory Manual," Center for Rotorcraft Education and Research, Univ. of Maryland, Tech. Rept. UM-AERO 94-18, College Park, July 1994.

[16]Shen, J., and Chopra, I., "A Parametric Design Study for a Swashplateless Helicopter Rotor with Trailing-Edge Flaps," *Journal of the American Helicopter Society*, Vol. 49, No. 1, 2004, pp. 43–53.

[17]Shen, J., Chopra, I., and Johnson, W., "Performance of Swashplateless Ultralight Helicopter Rotor with Trailing-Edge Flaps for Primary Flight Control," *American Helicopter Society 59th Annual Forum Proceedings*, American Helicopter Society, Alexandria, VA, 2003, p. 11.

[18]Shen, J., and Chopra, I., "Actuation Requirements of Swashplateless Trailing-Edge Flap Helicopter Rotor in Maneuvering and Autorotation Flights," *American Helicopter Society 60th Annual Forum Proceedings*, American Helicopter Society, Alexandria, VA, 2004.

[19]Datta, A., and Chopra, I., "Validation of Structural and Aerodynamic Modeling Using UH-60 Flight Test Data," *American Helicopter Society 59th Annual Forum Proceedings*, American Helicopter Society, Alexandria, VA, 2003, p. 15.

[20]Shen, J., and Chopra, I., "Ultralight Helicopter with Trailing-Edge Flap for Primary Control," *Proceedings of American Helicopter Society International Meeting on Advanced Rotorcraft Technology and Life Saving Activities*, American Helicopter Society, Alexandria, VA, 2002, p. 10.

[21]Shen, J., and Chopra, I., "Aeroelastic Stability of Trailing-Edge Flap Helicopter Rotors," *Journal of the American Helicopter Society*, Vol. 48, No. 4, 2003, pp. 236–243.

[22]Theodorsen, T., and Garrick, I. E., "Nonstationary Flow About a Wing-Aileron-Tab Combination Including Aerodynamic Balance," NACA Tech. Rept. 736, 1942.

[23]Johnson, W., "Self-Tuning Regulators for Multicyclic Control of Helicopter Vibration," NASA Tech. Rept. TP 1996, March 1982.

[24]Wei, F.-S. J., and Gallagher, F., "Servo-Flap Rotor Performance Flight Testing and Data Identification," *American Helicopter Society 57th Annual Forum Proceedings*, American Helicopter Society, Alexandria, VA, 2001, pp. 596–603.